Sea-ice drift characteristics revealed by measurement of acoustic Doppler current profiler and ice-profiling sonar off Hokkaido in the Sea of Okhotsk

Yasushi FUKAMACHI,[1] Kay I. OHSHIMA,[1] Yuji MUKAI,[2*] Genta MIZUTA,[2] Masaaki WAKATSUCHI[1]

[1]*Institute of Low Temperature Science, Hokkaido University, Sapporo 060-0819, Japan*
E-mail: yasuf@lowtem.hokudai.ac.jp
[2]*Graduate School of Environmental Science, Hokkaido University, Sapporo 060-0810, Japan*

ABSTRACT. In the southwestern part of the Sea of Okhotsk off Hokkaido, sea-ice drift characteristics are investigated using the ice and water velocities obtained from a moored upward-looking acoustic Doppler current profiler (ADCP) during the winters of 1999–2001. Using hourly-mean values of these data along with the wind data measured at a nearby coastal station, the wind factor and turning angle of the relative velocity between the ice and water velocities with respect to the wind are calculated assuming free drift under various conditions. Since the simultaneous sea-ice draft data are also available from a moored ice-profiling sonar (IPS), we examine the dependence of drift characteristics on ice thickness for the first time. As ice thickness increases and wind decreases, the wind factor decreases and the turning angle increases, as predicted by the theory of free drift. This study clearly shows the utility of the moored ADCP measurement for studying sea-ice drift, especially with the simultaneous IPS measurement for ice thickness, which cannot be obtained by other methods.

1. INTRODUCTION

There have been many studies of sea-ice motion since Nansen (1902). Ignoring internal ice stress, the steady-state balance of forces for sea-ice motion can be written (after Thorndike and Colony, 1982)

$$\boldsymbol{\tau}_a + \boldsymbol{\tau}_w + \boldsymbol{C} + \boldsymbol{T} = 0, \tag{1}$$

where

$$\boldsymbol{\tau}_a = \rho_a C_a |\boldsymbol{U}_a - \boldsymbol{U}_i| (\boldsymbol{U}_a - \boldsymbol{U}_i) e^{i\theta_a},$$
$$\boldsymbol{\tau}_w = \rho_w C_w |\boldsymbol{U}_w - \boldsymbol{U}_i| (\boldsymbol{U}_w - \boldsymbol{U}_i) e^{i\theta_w}.$$

Here $\boldsymbol{\tau}_a$ and $\boldsymbol{\tau}_w$ are wind and water stresses, $\boldsymbol{U}_i$, $\boldsymbol{U}_w$ and $\boldsymbol{U}_a$ are ice, water and wind velocities, ρ_i and ρ_w are ice and water densities, C_a and C_w are air and water drag coefficients, and θ_a and θ_w are the boundary-layer turning angles in air and water. $\boldsymbol{C}$ is the Coriolis force and $\boldsymbol{T}$ is the pressure-gradient force due to sea-surface tilt. Sea-ice motion governed by Equation (1) is called steady-state free drift. Considering the case with moderate to strong wind and thin ice, Thorndike and Colony (1982) examined the following relationship since the third and fourth terms in Equation (1) are relatively small:

$$\boldsymbol{U}_i = \alpha \boldsymbol{U}_a e^{-i\theta} + \overline{\boldsymbol{U}}_w + \boldsymbol{\varepsilon}, \tag{2}$$

where α is the wind factor, θ is the turning angle, $\boldsymbol{\varepsilon}$ is the residual and the overbar denotes the mean. Using daily geostrophic wind and ice velocity obtained from drifting buoys in the Arctic, they showed that >70% of the variance of the ice velocity is explained by the geostrophic wind, with a wind factor of 0.77% and a turning angle of 5° to the right of the wind. They also derived the mean ocean current from Equation (2) by subtracting the component of the ice motion caused by the wind from the total motion.

Recently, there have been many studies of sea-ice motion based on satellite remote-sensing data (e.g. Emery and others, 1997; Kwok and others, 1998; Kimura and Wakatsuchi, 2000). Kimura and Wakatsuchi (2000) carried out an analysis similar to Thorndike and Colony (1982) using the geostrophic wind and sea-ice motion derived from the daily Special Sensor Microwave/Imager (SSM/I) passive microwave data in all the sea-ice zones in the Northern Hemisphere. They showed that the wind factor and turning angle are larger in the seasonal sea-ice zones such as the Sea of Okhotsk (1.5% and 8.7°, respectively) than in the perennial ice zones such as the Arctic. They also derived the mean ocean current in a manner similar to Thorndike and Colony (1982).

Limitations of the studies based on buoy- or satellite-based sea-ice drift are the lack of water velocity data and typical time resolution being >1 day. Therefore, the temporal variability of ocean current cannot be isolated from ice motion in these studies. One method to obtain water velocity along with ice velocity at high temporal resolution is the in situ observation at a drifting ice station (e.g. Pease and Overland, 1984; Reynolds and others, 1985; Leppäranta and Omstedt, 1990; Martinson and Wamser, 1990). Reynolds and others (1985) used Argos-tracked floes with wind monitor and current meter to obtain sea-ice velocity at hourly intervals, and near-surface ocean and surface wind velocities at 30 min intervals in the Bering Sea marginal ice zone. They derived the ratio of air and water drag coefficients, C_a/C_w, in the range of 0.06–0.2. Since the wind factor, α, is roughly equal to the Nansen number $\sqrt{(\rho_a C_a)/(\rho_w C_w)}$, these values correspond to a wind factor of ~0.88–1.61%.

Another method for obtaining water velocity along with ice velocity is the mooring measurement of the

*Present address: Kobe Marine Observatory, Japan Meteorological Agency, Kobe 651-0073, Japan.

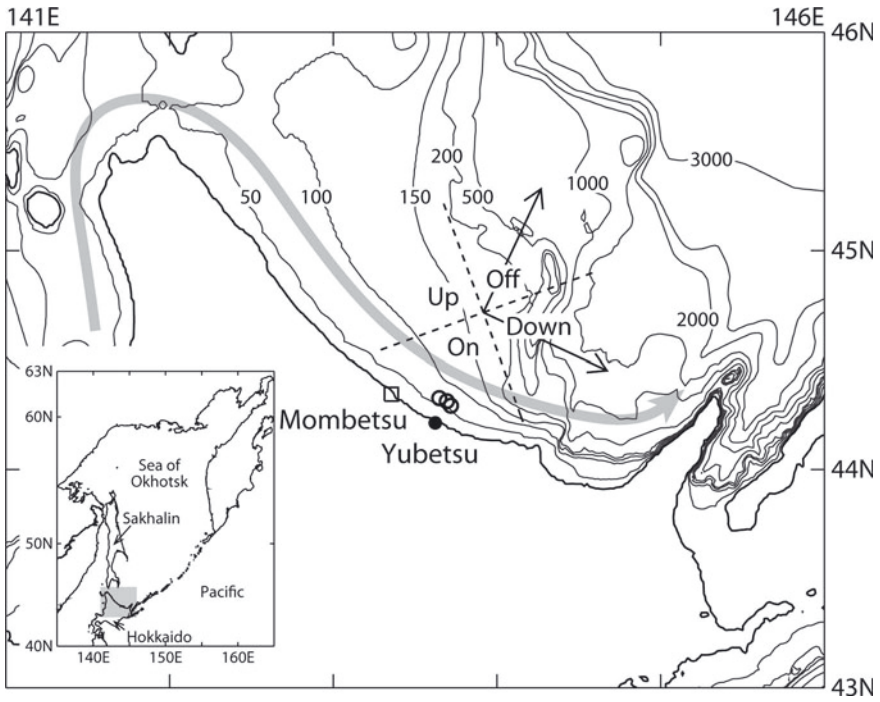

Fig. 1. Map showing the locations of the moorings (denoted by open circles). The three locations, from northwest to southeast, were for 1999, 2000 and 2001, respectively. The surface-wind data were measured in Yubetsu (solid circle). The alongshore and offshore directions, and the boundaries of the four different wind directions (see Table 2) are indicated by black arrows and dashed lines, respectively. The atmospheric pressure data and the sea-ice radar data were obtained in Mombetsu (square). The Soya Warm Current is schematically shown by the gray arrow. The inset map shows the entire Sea of Okhotsk. The shading denotes the region of the enlarged map. Bathymetry data (in m) are extracted from the General Bathymetric Chart of the Oceans.

upward-looking acoustic Doppler current profiler (ADCP). The ADCP has two modes of measurement: the water-track mode to measure water velocity and the bottom-track mode to measure ship speed for the ship-mounted downward-looking ADCP. Belliveau and others (1990) showed that this bottom-track mode of the upward-looking ADCP can be used to measure sea-ice velocity. This measurement method has been used in many mooring observations in the sea-ice zones, mostly with ice-profiling sonar (IPS) to measure sea-ice draft (e.g. Melling and Riedel, 1995, 1996; Melling and others, 1995, 2005; Fukamachi and others, 2003, 2006, 2009). In these studies, sea-ice velocity data are mainly used to convert sea-ice draft time series to spatial series, and sea-ice drift itself was not fully examined. This method can obtain a large number of data under a variety of conditions relatively easily, and is capable of examining the data for a variety of ice thickness provided that sea-ice draft is obtained by IPS simultaneously. These are advantages of this Eulerian measurement over the Lagrangian drifting ice-station measurement.

In this study, we use hourly-mean velocities of both ice and water obtained by the moored upward-looking ADCP off Hokkaido in the Sea of Okhotsk during the winters of 1999–2001. Using these data along with the wind data measured at the coast, we examine how sea-ice drift characteristics change depending on wind. In addition, we examine the dependence of sea-ice drift on ice thickness using the draft data obtained by the moored IPS along with the ADCP. Although we use the hourly-mean data to take full advantage of a large number of data at a fine temporal resolution, we assume the steady-state free drift as a dynamical framework for simplicity in the following analyses. The fact that the relative ice velocity and wind have the maximum correlation without any lag (as described in section 4) provides support for considering the steady-state balance.

2. DATA AND PROCESSING

Before the data used in this study are discussed, the general ice conditions in the Sea of Okhotsk are briefly summarized here. Sea ice first forms near the northern and northwestern coasts in November, then spreads southward along Sakhalin and eventually reaches Hokkaido typically by mid-January. Maximum ice extent normally occurs in early March. Finally, it retreats from Hokkaido in early April. The average sea-ice concentration in the 60 km radius area from Mombetsu (square in Fig. 1) observed by a sea-ice radar was 60%, 68% and 63% during the ice observation periods at the moorings (listed in Table 1) in 1999, 2000 and 2001, respectively (Ishikawa and others, 2001). Both sea-ice arrival at, and retreat from, the coast of Hokkaido occurred later than, around and earlier than the normal time in 1999, 2000 and 2001, respectively (JMA, 2001).

To avoid fishing activities, the moorings were deployed at slightly different locations in the three years (Fig. 1; Table 1). They were located ~11 km off the northeastern coast of Hokkaido, where the water is 56–59 m deep. Thus, the region of observation is located at the southern end of the ice coverage in this sea. The mean ice thickness obtained in 1999–2001 was 0.71 m (Fukamachi and others, 2006). A coastal current, the Soya Warm Current, flows to the east-southeast in this region even in winter (Ebuchi and others, 2006; Fukamachi and others, 2008). The moorings contained an ADCP (RD Instruments WH-Sentinel 300 kHz) moored ~13.5 m above the ocean bottom. The ADCP

measured ice velocity using the bottom-track mode as well as water-column velocity uing the water-track mode (Belliveau and others, 1990; Melling and others, 1995). Its sampling interval was 15 min and the bin size for water-column velocity was 4 m. In this study, we use hourly-mean ice velocity and near-surface velocity in the uppermost valid bin (Table 1). The accuracy of the speed is $<1\,\mathrm{cm\,s^{-1}}$.

Since wind was not measured at the mooring site, we used wind data obtained every 10 min at the Japan Meteorological Agency's nearby station in Yubetsu (solid circle in Fig. 1). The measurement height is 9.4 m above the ground (14.4 m a.s.l.). Hourly-mean wind data are calculated from the 10 min data. We use the alongshore and offshore components of all the velocities obtained by rotating 25° clockwise to align the alongshore component with the coast in the following analyses (Fig. 1).

Another mooring with an IPS (ASL Environmental Sciences IPS4 420 kHz) was also deployed, ~300 m apart from the ADCP mooring to avoid possible acoustic interference. The IPS was moored ~14 m above the ocean bottom. With this instrument depth, it viewed a spot of ~2 min diameter at the surface. The IPS sampling intervals were 1 s for range and echo-amplitude data and 1 min for pressure and tilt data. The representative accuracy of the draft is about ±0.05 m. In this study, we use hourly-mean thickness converted from draft (ice thickness below the water surface) assuming isostasy, and water and ice densities of 1026 and $876\,\mathrm{kg\,m^{-3}}$ (Toyota and others, 2007), respectively. The draft data at 1 s intervals were calculated from the IPS data, along with the atmospheric pressure data obtained at the nearby meteorological station in Mombetsu (square in Fig. 1) by Fukamachi and others (2006). To select the hourly-mean ice velocity during good ice coverage, in the following analyses we exclude data obtained when sea ice was not observed for >30 min within each hour.

Table 1. Mooring information

	Year		
	1999	2000	2001
Mooring period	5 Dec 1998 to 27 Mar 1999	12 Dec 1999 to 4 Apr 2000	26 Nov 2000 to 22 Mar 2001
Location	44°19.6′ N, 143°39.2′ E	44°18.8′ N, 143°41.8′ E	44°17.6′ N, 143°43.1′ E
Water depth (m)	~56	~59	~59
ADCP depth (m)	~43	~45	~45
ADCP topmost layer (m)	~3–7	~5–9	~5–9
Ice observation period	9 Feb–27 Mar (47 days)	23 Jan–1 Apr (70 days)	6 Jan–21 Mar (75 days)

3. METHODS

We obtain ocean velocity, $\boldsymbol{U}_\mathrm{w}$, as well as ice ($\boldsymbol{U}_\mathrm{i}$) and wind ($\boldsymbol{U}_\mathrm{a}$) velocities, so Equation (2) becomes

$$\boldsymbol{U}_\mathrm{i} - \boldsymbol{U}_\mathrm{w} = \alpha \boldsymbol{U}_\mathrm{a} \mathrm{e}^{-i\theta} + \boldsymbol{\varepsilon},$$

where θ is the turning angle between the wind-driven ice drift and wind. This equation can be written as

$$\begin{bmatrix} U_\mathrm{i} - U_\mathrm{w} \\ V_\mathrm{i} - V_\mathrm{w} \end{bmatrix} = \alpha \begin{bmatrix} \cos\theta & \sin\theta \\ -\sin\theta & \cos\theta \end{bmatrix} \begin{bmatrix} U_\mathrm{a} \\ V_\mathrm{a} \end{bmatrix} + \begin{bmatrix} \varepsilon_u \\ \varepsilon_v \end{bmatrix}, \quad (3)$$

where U and V denote the alongshore and across-shore components. We assume that the surface wind, $\boldsymbol{U}_\mathrm{a}$, and near-surface water velocity, $\boldsymbol{U}_\mathrm{w}$, act on the ice surface and bottom.

The turning angle, θ, and wind factor, α, can be obtained by a least-squares method to minimize $S = \sum_{k=1}^{n} \boldsymbol{\varepsilon}^2(k) = \sum_{k=1}^{n} (\varepsilon_u^2(k) + \varepsilon_v^2(k))$. Letting $\boldsymbol{U}_\mathrm{iw} \equiv \boldsymbol{U}_\mathrm{i} - \boldsymbol{U}_\mathrm{w}$ and following Kimura and Wakatsuchi (2000), they are

$$\theta = \arctan\left[\frac{\sum_{k=1}^{n}\{V_\mathrm{a}(k)\,U_\mathrm{iw}(k)\} - \sum_{k=1}^{n}\{U_\mathrm{a}(k)\,V_\mathrm{iw}(k)\}}{\sum_{k=1}^{n}\{U_\mathrm{a}(k)\,U_\mathrm{iw}(k)\} + \sum_{k=1}^{n}\{V_\mathrm{a}(k)\,V_\mathrm{iw}(k)\}}\right] \quad (4)$$

and

$$\alpha = \frac{c_1 + c_2 - c_3 + c_4}{\sum_{k=1}^{n} U_\mathrm{a}^2(k) + \sum_{k=1}^{n} V_\mathrm{a}^2(k)}, \quad (5)$$

where

$$c_1 = \cos\theta \sum_{k=1}^{n} \{U_\mathrm{a}(k)\,U_\mathrm{iw}(k)\},$$

$$c_2 = \sin\theta \sum_{k=1}^{n} \{V_\mathrm{a}(k)\,U_\mathrm{iw}(k)\},$$

$$c_3 = \sin\theta \sum_{k=1}^{n} \{U_\mathrm{a}(k)\,V_\mathrm{iw}(k)\},$$

$$c_4 = \cos\theta \sum_{k=1}^{n} \{V_\mathrm{a}(k)\,V_\mathrm{iw}(k)\}.$$

After Kimura and Wakatsuchi (2000), the goodness of the fit can be estimated by the correlation coefficient, r, calculated from

$$r = \frac{c_1 + c_2 - c_3 + c_4}{\sqrt{\sum_{k=1}^{n} U_\mathrm{a}^2(k) + \sum_{k=1}^{n} V_\mathrm{a}^2(k)}\sqrt{\sum_{k=1}^{n} U_\mathrm{iw}^2(k) + \sum_{k=1}^{n} V_\mathrm{iw}^2(k)}}. \quad (6)$$

In the next section, we examine sea-ice drift characteristics based on θ, α and r.

4. RESULTS

The ice and ocean velocities (Fig. 2a and b) and the relative velocity between the ice and ocean velocities and wind (Fig. 2c and d) during 2000 are shown as examples. Only the alongshore components of the relative velocity and wind during 1999 and 2001 are also shown in Figure 3a and c. The ocean velocity is essentially the combination of the Soya Warm Current to the east-southeast and diurnal tidal currents mostly in the alongshore direction (Odamaki, 1994). The ice and ocean velocities correspond fairly well (Fig. 2a and b). Their correlation coefficients are 0.79 and 0.71 for the alongshore and across-shore components, respectively.

A lag-correlation analysis shows that the relative velocity between the ice and ocean velocities, and wind have the maximum correlation coefficient without any lag. However, they do not correspond as well as the ice and ocean velocities do (Figs 2c and d and 3a and c). Their correlation coefficients are 0.66 and 0.54 for the alongshore and across-shore components, respectively. Figure 2d, in particular, shows that the across-shore component of the relative velocity does not correspond well with the wind directed offshore. This difference is likely caused by the difference between the wind at the coastal station and that at the mooring site, namely, the wind data obtained in

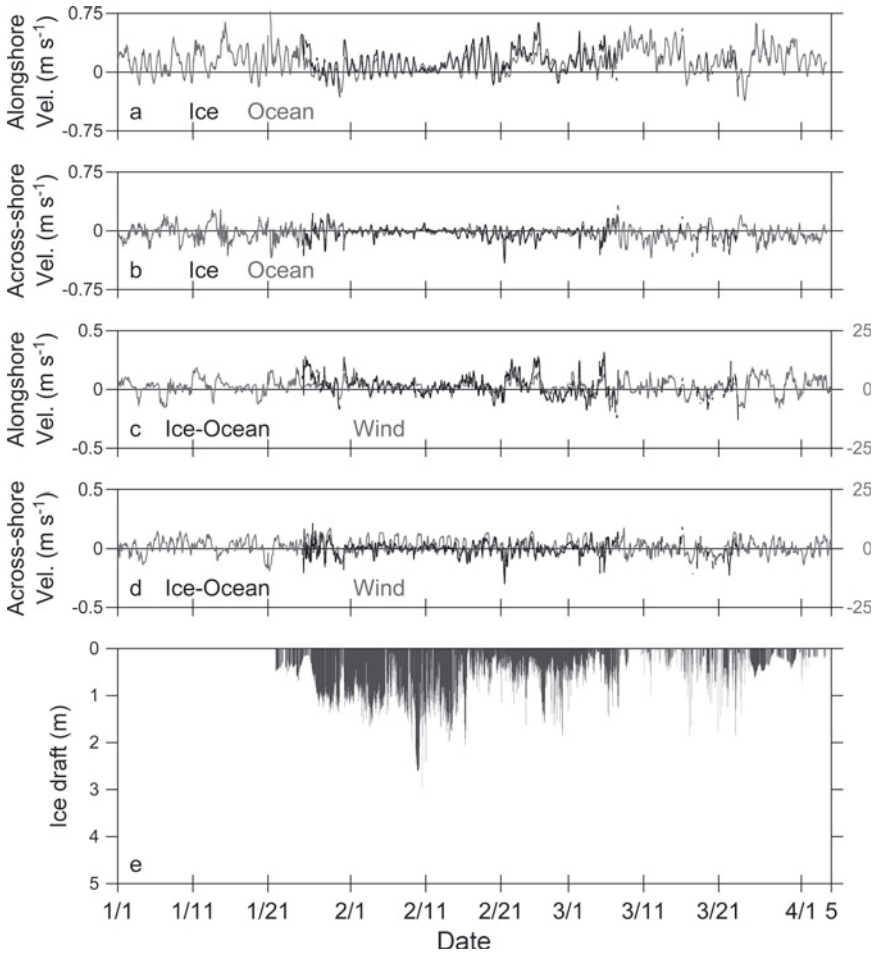

Fig. 2. (a) Hourly-mean alongshore and (b) across-shore components of ice (black) and ocean (gray) velocities, and (c) alongshore and (d) across-shore components of the relative velocity between ice and ocean (black), and wind (gray) in 2000. Dates are month/day. Note that the scales for the relative velocity (left) and wind (right) are different and the full scale is 50 times larger for the wind. (e) Hourly-mean ice draft calculated from >30 min (<30 min) ice data is shown in black (gray). Note that periods of valid ice–ocean velocity and ice-thickness data do not always match because of their different measurement modes and intervals (burst at every 15 min for the ADCP and continuous at every 1 s for the IPS).

Yubetsu are affected by the diurnal land breeze, which is likely weaker at the offshore mooring site. In fact, the wind data of the European Centre for Medium-Range Weather Forecasts (ECMWF) at the nearby gridpoint (45° N, 144° E; ~82 km offshore from the mooring site) in 1999 have fewer instances of the offshoreward wind. Correlation coefficients of these two wind data based on the 6 hourly data of the ECMWF data interval are 0.71 and 0.52 for the alongshore and across-shore components, respectively. The high correlation coefficient for the alongshore component indicates that the coastal wind represents the marine wind relatively well in this direction, but the low value for the across-shore component does not. The correlation coefficients between the ECMWF wind and the relative ice velocities are low at 0.20 and 0.46 for the alongshore and across-shore components, respectively. For these reasons and because of the fine temporal resolution (1 hour) of the wind in Yubetsu, we use the wind data measured at the coast in the following analyses. Based on all the data (2582 over the three winters), the turning angle, θ, wind factor, α, and correlation coefficient, r, calculated by Equations (4–6) are 9.4° (to the right of the wind direction), 1.59% and 0.54, respectively.

4.1. Dependence on wind direction

Since the wind directed offshore is affected by the local land breeze, we first examine the dependence of the drift characteristics on wind direction. The wind data are separated into four cases: the offshore-, downstream-, onshore- and upstreamward directions (Fig. 1). The offshoreward wind is defined as wind with its direction in a 90° range, with the offshoreward direction (25° clockwise from the north) at its center. The downstreamward (upstreamward) wind range has its center roughly in the east-southeast (west-northwest) direction.

The wind factor and correlation coefficient are quite different for the offshoreward wind case (Table 2). They are much smaller than for the other cases, indicating that the wind speed is stronger at the coast than at the mooring site and the relative ice velocity cannot be expressed well by the coastal wind. Also, the wind factor and correlation coefficient for the onshoreward wind case are smaller than for the downstream- and upstreamward wind cases. This suggests that the internal ice stress is more important for the case with the onshoreward wind which advects sea ice towards the coast, especially because the mooring sites were near the coast. For these reasons, we exclude the data

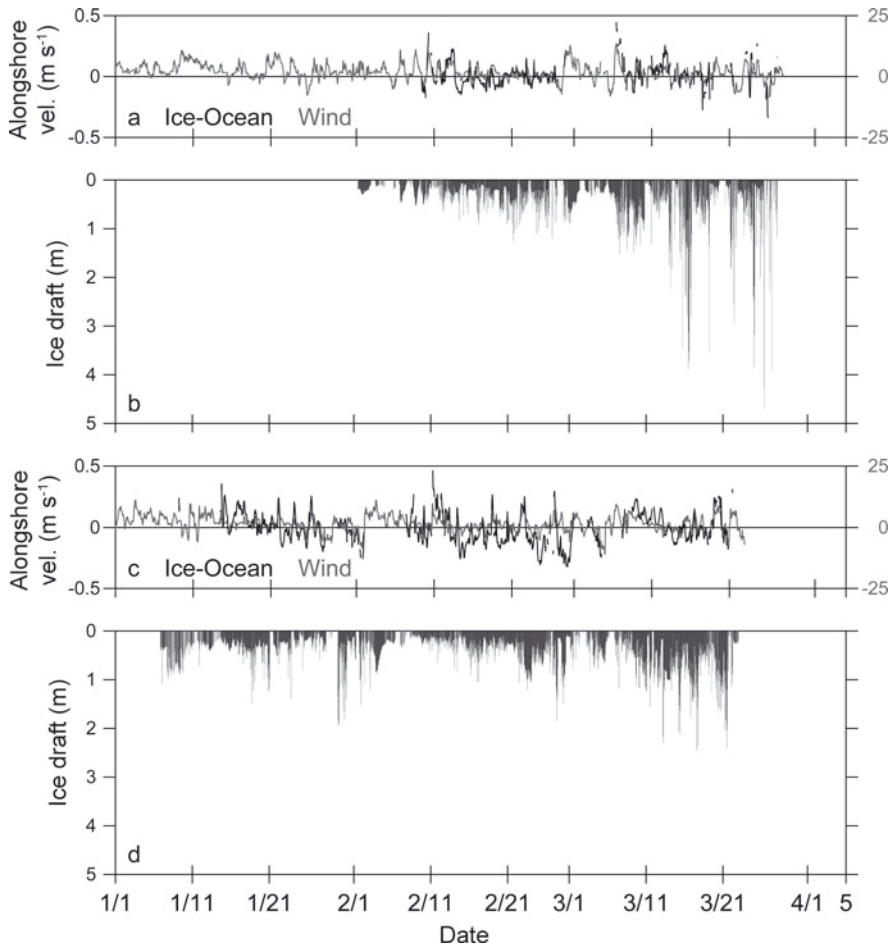

Fig. 3. Hourly-mean alongshore components of the relative ice velocity (black) and wind (gray) in (a) 1999 and (c) 2001. Also shown is hourly-mean ice draft in (b) 1999 and (d) 2001. Dates are month/day.

with the across-shore wind from the following analyses and concentrate on the data with the alongshore wind, which is more reliable at the coast. (For the tables, however, we also retain the drift characteristics based on the wind data in all directions.)

4.2. Dependence on wind speed

Equation (3) is derived from Equation (1) assuming the conditions with moderate to strong wind so that the Coriolis and pressure-gradient terms are comparably smaller than the wind and water stresses. As expected from this assumption, the correlation coefficient increases as the wind increases for wind speed more than $2\,m\,s^{-1}$ (Table 3), indicating that the relative ice velocity is better expressed by the wind. Note that the turning angle decreases and the wind factor increases as the wind speed increases as shown by the previous theoretical studies (Gaskill and others, 1980; Thorndike and Colony, 1982; Pease and Overland, 1984; Leppäranta, 1998, 2005). Since the correlation coefficient is <0.4 for the data with wind speed $<2\,m\,s^{-1}$, we exclude these data from the following analyses.

4.3. Dependence on sea-ice thickness

Since the simultaneous ice-thickness data are available from the IPS, we also examine the dependence of sea-ice drift characteristics on ice thickness. This analysis is not possible for other observational methods such as buoy- or satellite-based remote sensing and drifting ice station. The turning angle increases and the wind factor decreases as ice thickness increases for the ranges larger than 0.5 m (Table 4). This is because the Coriolis force becomes more important and ice–water drag increases as ice thickness increases. These tendencies agree with the results of the previous theoretical studies (Gaskill and others, 1980; Pease and Overland, 1984; Leppäranta, 1998, 2005).

5. DISCUSSIONS AND SUMMARY

The free-drift balance expressed by Equation (3) is most applicable for the case with strong wind and small ice thickness, so the wind factor of 2.68% (defined as α_0) is

Table 2. Sea-ice drift characteristics for different wind directions during 1999–2001

	Wind direction				
	Offshore-ward	Downstream-ward	Onshore-ward	Upstream-ward	Alongshore*
Data	1172	768	252	390	1158
θ (°)	7.8	10.4	24.0	1.0	8.3
α (%)	0.77	2.29	2.16	2.98	2.41
r	0.34	0.70	0.59	0.73	0.70

*Combined data of the downstream and upstream directions.

Table 3. Sea-ice drift characteristics for different ranges of wind speed during 1999–2001. Both values for the alongshore wind direction and all the wind directions (in parentheses) are listed

	Wind speed				
	0–2 m s^{-1}	2–4 m s^{-1}	4–6 m s^{-1}	≥6 m s^{-1}	≥2 m s^{-1}
Data	265 (575)	434 (952)	292 (682)	167 (373)	893 (2007)
θ (°)	–4.6 (–23.6)	11.5 (11.2)	8.6 (13.1)	7.8 (8.0)	8.7 (10.4)
α (%)	2.62 (1.85)	1.94 (1.39)	2.51 (1.55)	2.51 (1.72)	2.40 (1.59)
r	0.37 (0.28)	0.50 (0.39)	0.77 (0.58)	0.84 (0.71)	0.73 (0.58)

calculated from the data with wind speed >6 m s^{-1} and thickness 0–0.5 m. (The turning angle and correlation coefficient are 9.1° and 0.84, respectively.) Using the ratio of surface wind to geostrophic wind of 0.5–0.7 in near-neutral conditions over sea ice (Leppäranta, 2005), the wind factor of 1.5% derived by Kimura and Wakatsuchi (2000) in the Sea of Okhotsk with geostrophic wind corresponds to 2.1–3.0% with surface wind. The value of 2.68% is also within the range (2.5–3.0%) obtained in the Baltic Sea with surface wind (Leppäranta and Omstedt, 1990).

Since the drag coefficients between air and ice, and ice and water are important factors for transferring momentum among them and crucial parameters in numerical models, there have been many observational studies of these drag coefficients in various ice-covered oceans (e.g. Overland, 1985; Martinson and Wamser, 1990; Guest and Davidson, 1991). In the Sea of Okhotsk, however, there have been a few observational studies (e.g. Shirasawa and Aota, 1991; Fujisaki and others, 2009). Fujisaki and others (2009) measured the air–ice drag coefficient, C_a, from an ice-breaker off Hokkaido and derived a value of 2.7–3.1 × 10^{-3}. As described in section 1, the evaluation of the wind factor is roughly equivalent to that of the ratio between the air and water drag coefficients, C_a/C_w. Thus, we can estimate the water drag coefficient, which is more difficult to measure, from combining our results and those of Fujisaki and others (2009). Using the wind factor $\alpha_0 = 2.68\%$ defined above, C_w is estimated to be 4.5–5.1 × 10^{-3}. These are larger values than that of 3.5 × 10^{-3} in the Baltic Sea (Leppäranta and Omstedt, 1990) and close to those of 5.0 × 10^{-3} in the Beaufort Sea (McPhee, 1982) and 5.4 × 10^{-3} in the Barrow Strait (Shirasawa and Ingram, 1991).

For thick ice and/or weak wind, we need to retain the Coriolis and pressure-gradient terms in Equation (1). Gaskill and others (1980), and Pease and Overland (1984) calculated the wind factor and turning angle for varying ice thickness and wind speed in their theoretical studies. Leppäranta (1998, 2005) derived the equations for the wind factor, α, and turning angle, θ, for this case. They are

$$\alpha^4 + 2\sin\theta_w\, R\,\alpha_0^2\,\alpha^3 + R^2\,\alpha_0^4\,\alpha^2 - \alpha_0^4 = 0, \quad (7)$$

$$\tan(\theta + \theta_a) = \tan\theta_w + \alpha_0^2\, R/(\alpha\cos\theta_w). \quad (8)$$

Here R is a dimensionless quantity defined as $R = (\rho_i h_i f)/(\rho_a C_a U_a)$, where ρ_i and h_i are ice density and

Table 4. Sea-ice drift characteristics for different ranges of ice thickness during 1999–2001. Both values for the alongshore wind direction and all the wind directions (in parentheses) are listed. The data are limited for wind speed >2 m s^{-1}

	Ice thickness			
	0–0.5 m	0.5–1.0 m	1.0–1.5 m	>1.5 m
Data	406 (898)	276 (598)	159 (363)	52 (148)
θ (°)	11.4 (8.9)	5.5 (7.3)	7.7 (16.3)	11.8 (30.6)
α (%)	2.48 (1.65)	2.53 (1.81)	2.12 (1.42)	1.66 (0.83)
r	0.71 (0.54)	0.80 (0.65)	0.70 (0.61)	0.60 (0.47)

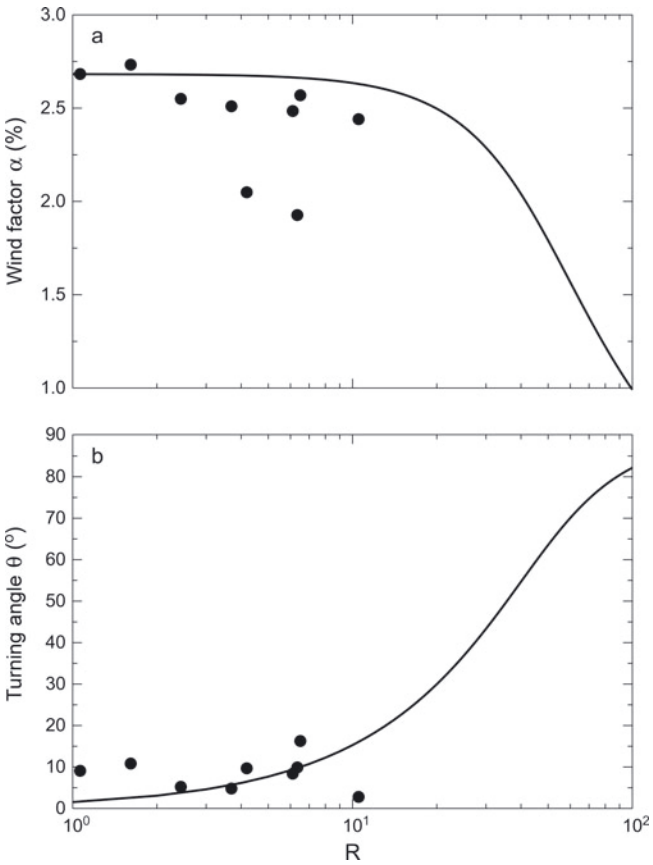

Fig. 4. Curves of (a) the wind factor, α, and (b) turning angle, θ, against R derived from Equations (7) and (8) when $\theta_a = \theta_w = 0$. Circles are values obtained from the data for the cases with different combinations of wind-speed and ice-thickness ranges. The ranges are the same as those shown in Tables 3 and 4. Only values obtained when the correlation coefficient, r, is >0.6 are plotted. R is calculated using $C_a = 2.7 \times 10^{-3}$ after Fujisaki and others (2009). Note that the R-axis is drawn in a logarithmic scale for clarity.

thickness and f is the Coriolis parameter. Thus, R is a measure of the importance of the Coriolis and pressure-gradient terms and it increases as ice thickness increases and wind speed decreases. Since we assume that the surface wind and near-surface water velocity used in this study act on the ice surface and bottom, we set $\theta_a = \theta_w = 0$ in these equations. Figure 4 shows the wind factor and turning angle in this case with $\alpha_0 = 2.68\%$. The curves in Figure 4 show that the wind factor decreases and the turning angle increases as R increases. Also plotted by circles are the wind factors and turning angles obtained from the present dataset. Their values are calculated from the part of the dataset with different combinations of wind-speed and ice-thickness ranges shown in Tables 3 and 4, respectively. Values of R are determined from these combinations along with $C_a = 2.7 \times 10^{-3}$ after Fujisaki and others (2009). Although there are some outliers, these results generally follow the theoretical curves from Equations (7) and (8). The wind factor decreases and the turning angle increases as R increases. The smaller wind factors than the theoretical values may be due to the effect of internal ice stress. Although the range of R is somewhat limited mainly due to the absence of thick ice, our dataset is a rare example of the dependence of drift characteristics on the combination of ice thickness and wind speed, and their resulting agreement with the theory. This is because it is not possible to collect sea-ice drift data along with thickness data (of a variety of thickness) by other methods such as remote-sensing and drifting-station observations.

This study clearly shows the utility of the moored ADCP measurement for studying sea-ice drift. This method is especially effective if the moored measurement of ice draft is carried out simultaneously. Limitations of this study are the assumption of steady-state balance and the quality of the across-shore wind data. The assumption of steady-state balance for the hourly-mean ice drift over the mooring is a rather simplified approach. The validity of this assumption cannot be tested strictly based on the available dataset and this remains an issue. However, the fact that the wind factor and turning angle change consistently with the theory may provide another support for considering the steady-state balance. The use of the objectively analyzed wind data, which are presumably free of land–sea breeze, with high temporal and spatial resolutions such as the Grid Point Value data produced by the Japanese Meteorological Agency (only available since October 2003) would enable us to examine sea-ice drift for all the wind directions.

ACKNOWLEDGEMENTS

We are deeply indebted to H. Melling and D. Fissel for their advice concerning the observations. Logistical support was provided by the Yubetsu Fishermen's Union, Sanyo-Techno Marine Inc. and the Sea Ice Research Laboratory of Hokkaido University. We thank T. Takatsuka for data processing. Discussions with M. Kawashima and T. Toyota were helpful. Figures were produced by the PSPLOT Libraries written by K.E. Kohler, and Figure 1 was drawn by K. Kitagawa. This work was supported by funds from the Core Research for Evolutional Science and Technology of the Japan Science and Technology Corporation, and from Grants-in-Aid 12740266, 17540405 and 20221001 for scientific research from the Ministry of Education, Science, Sports, and Culture of Japan.

REFERENCES

Belliveau, D.J., G.L. Bugden, B.M. Eid and C.J. Calnan. 1990. Sea ice velocity measurements by upward-looking Doppler current profilers. *J. Atmos. Oceanic Technol.,* **7**(4), 596–602.

Ebuchi, N. *and 7 others.* 2006. Observation of the Soya Warm Current using HF ocean radar. *J. Oceanogr.,* **62**(1), 47–61.

Emery, W.J., C.W. Fowler and J.A. Maslanik. 1997. Satellite-derived maps of Arctic and Antarctic sea-ice motion. *Geophys. Res. Lett.,* **24**(8), 897–900.

Fujisaki, A., H. Yamaguchi, T. Takenobu, A. Futatsudera and M. Miyanaga. 2009. Measurements of air–ice drag coefficient over the ice-covered Sea of Okhotsk. *J. Oceanogr.,* **65**(4), 487–498.

Fukamachi, Y., G. Mizuta, K.I. Ohshima, H. Melling, D. Fissel and M. Wakatsuchi. 2003. Variability of sea-ice draft off Hokkaido in the Sea of Okhotsk revealed by a moored ice-profiling sonar in winter of 1999. *Geophys. Res. Lett.,* **30**(7), 1376. (10.1029/2002GL016197.)

Fukamachi, Y., G. Mizuta, K.I. Ohshima, T. Toyota, N. Kimura and M. Wakatsuchi. 2006. Sea ice thickness in the southwestern Sea of Okhotsk revealed by a moored ice-profiling sonar. *J. Geophys. Res.,* **111**(C9), C09018. (10.1029/2005JC003327.)

Fukamachi, Y. *and 7 others.* 2008. Volume transport of the Soya Warm Current revealed by bottom-mounted ADCP and ocean-radar measurement. *J. Oceanogr.,* **64**(3), 385–392.

Fukamachi, Y. *and 7 others.* 2009. Direct observations of sea-ice thickness and brine rejection off Sakhalin in the Sea of Okhotsk. *Continental Shelf Res.,* **29**(11–12), 1541–1548.

Gaskill, H.S., R.J. Lopez and G.E. Swaters. 1980. *Free drift of sea ice: a comparison of models.* St John's, Memorial University of Newfoundland. Centre for Cold Ocean Resources Engineering. (C-CORE Tech. Rep. 80-16.)

Guest, P.S. and K.L. Davidson. 1991. The aerodynamic roughness of different types of sea ice. *J. Geophys. Res.,* **96**(C3), 4709–4721.

Ishikawa, M., T. Takatsuka, T. Daibou, K. Shirasawa and M. Aota. 2001. Distributions of pack ice in the Okhotsk Sea off Hokkaido observed using a sea-ice radar network, January–April, 2001. *Low Temp. Sci., Ser. A* 60, 13–40.

Japanese Meteorological Agency (JMA). 2001. *The results of sea ice observations, No. 19.* Tokyo, Japanese Meteorological Agency. CD-ROM.

Kimura, N. and M. Wakatsuchi. 2000. Relationship between sea-ice motion and geostrophic wind in the Northern Hemisphere. *Geophys. Res. Lett.,* **27**(22), 3735–3738.

Kwok, R., A. Schweiger, D.A. Rothrock, S. Pang and C. Kottmeier. 1998. Sea ice motion from satellite passive microwave imagery assessed with ERS SAR and buoy motions. *J. Geophys. Res.,* **103**(C4), 8191–8214.

Leppäranta, M. 1998. The dynamics of sea ice. *In* Leppäranta, M., *ed. Physics of ice-covered seas.* Helsinki, University of Helsinki Press, 305–342.

Leppäranta, M. 2005. *The drift of sea ice.* Berlin, etc., Springer-Verlag.

Leppäranta, M. and A. Omstedt. 1990. Dynamic coupling of sea ice and water for an ice field with free boundaries. *Tellus,* **42A**(4), 482–495.

McPhee, M.G. 1982. Sea ice drag laws and simple boundary layer concepts, including application to rapid melting. *CRREL Rep.* 82-4.

Martinson, D.G. and C. Wamser. 1990. Ice drift and momentum exchange in winter Antarctic pack ice. *J. Geophys. Res.,* **95**(C2), 1741–1755.

Melling, H. and D.A. Riedel. 1995. The underside topography of sea ice over the continental shelf of the Beaufort Sea in the winter of 1990. *J. Geophys. Res.,* **100**(C7), 13,641–13,653.

Melling, H. and D.A. Riedel. 1996. Development of seasonal pack ice in the Beaufort Sea during the winter of 1991–1992: a view from below. *J. Geophys. Res.,* **101**(C5), 11,975–11,991.

Melling, H., P.H. Johnston and D.A. Riedel. 1995. Measurements of the underside topography of sea ice by moored subsea sonar. *J. Atmos. Oceanic Technol.,* **12**(3), 589–602.

Melling, H., D.A. Riedel and Z. Gedalof. 2005. Trends in the draft and extent of seasonal pack ice, Canadian Beaufort Sea. *Geophys. Res. Lett.,* **32**(24), L24501. (10.1029/2005GL024483.)

Nansen, F. 1902. *The oceanography of the North Polar Basin. Norwegian North Polar Expedition 1893–1896. Scientific Results. Vol. III, No. IX, 1899–1902*. Christiana, Jacob Dybwad/London, etc., Longmans, Green.

Odamaki, M. 1994. Tides and tidal currents along the Okhotsk coast of Hokkaido. *J. Oceanogr.,* **50**(3), 265–279.

Overland, J.E. 1985. Atmospheric boundary layer structure and drag coefficients over sea ice. *J. Geophys. Res.*, **90**(C5), 9029–9049

Pease, C.H. and J.E. Overland. 1984. An atmospherically driven sea-ice drift model for the Bering Sea. *Ann. Glaciol.,* **5**, 111–114.

Reynolds, M., C.H. Pease and J.E. Overland. 1985. Ice drift and regional meteorology in the southern Bering Sea: results from MIZEX West. *J. Geophys. Res.,* **90**(C6), 11,967–11,981.

Shirasawa, K. and M. Aota. 1991. Atmospheric boundary layer measurements over sea ice in the Sea of Okhotsk. *J. Mar. Syst.,* **2**(1–2), 63–79.

Shirasawa, K. and R.G. Ingram. 1991. Characteristics of the turbulent oceanic boundary layer under sea ice. Part 1: a review of the ice–ocean boundary layer. *J. Mar. Syst.,* **2**(1), 153–160.

Thorndike, A.S. and R. Colony. 1982. Sea ice motion in response to geostrophic winds. *J. Geophys. Res.,* **87**(C8), 5845–5852.

Toyota, T., S. Takatsuji, K. Tateyama, K. Naoki and K.I. Ohshima. 2007. Properties of thick sea ice and overlying snow in the southern Sea of Okhotsk. *J. Oceanogr.,* **63**(3), 393–411.